Brain Imaging and Behavior (2019) 13:408–420
https://doi.org/10.1007/s11682-018-9864-6

ORIGINAL RESEARCH

Presurgical localization and spatial shift of resting state networks in patients with brain metastases

Ju-Rong Ding[1,2] · Fangmei Zhu[3] · Bo Hua[1] · Xingzhong Xiong[1] · Yuqiao Wen[1] · Zhongxiang Ding[3] · Paul M. Thompson[2]

Published online: 2 April 2018

Abstract

Brain metastases are the most prevalent cerebral tumors. Resting state networks (RSNs) are involved in multiple perceptual and cognitive functions. Therefore, precisely localizing multiple RSNs may be extremely valuable before surgical resection of metastases, to minimize neurocognitive impairments. Here we aimed to investigate the reliability of independent component analysis (ICA) for localizing multiple RSNs from resting-state functional MRI (rs-fMRI) data in individual patients, and further evaluate lesion-related spatial shifts of the RSNs. Twelve patients with brain metastases and 14 healthy controls were recruited. Using an improved automatic component identification method, we successfully identified seven common RSNs, including: the default mode network (DMN), executive control network (ECN), dorsal attention network (DAN), language network (LN), sensorimotor network (SMN), auditory network (AN) and visual network (VN), in both individual patients and controls. Moreover, the RSNs in the patients showed a visible spatial shift compared to those in the controls, and the spatial shift of some regions was related to the tumor location, which may reflect a complicated functional mechanism - functional disruptions and reorganizations - caused by metastases. Besides, higher cognitive networks (DMN, ECN, DAN and LN) showed significantly larger spatial shifts than perceptual networks (SMN, AN and VN), supporting a functional dichotomy between the two network groups even in pathologic alterations associated with metastases. Overall, our findings provide evidence that ICA is a promising approach for presurgical localization of multiple RSNs from rs-fMRI data in individual patients. More attention should be paid to the spatial shifts of the RSNs before surgical resection.

Keywords Brain metastases · Resting state networks · Independent component analysis · Resting-state functional MRI

Introduction

Brain metastases are the most prevalent cerebral tumors in adults; they often arise from lung and breast tumors (Gavrilovic and Posner 2005). With the improvements in detection and treatment of primary cancers, the incidence of brain metastases appears to be increasing (Lin and DeAngelis 2015). Around 70–80% of patients have less than three metastases (Delattre et al. 1988), and in this case, surgical resection is generally considered as a valid treatment to extend survival time (Sills 2005). Nevertheless, surgical resection of metastases has a risk of neurocognitive impairments caused by damage to functionally critical areas. To optimize resection of the tumor tissue while maintaining essential brain functions, precise localization of eloquent functional areas is of the utmost importance for presurgical planning (Sunaert 2006).

Electronic supplementary material The online version of this article (https://doi.org/10.1007/s11682-018-9864-6) contains supplementary material, which is available to authorized users.

✉ Ju-Rong Ding
jurongding@gmail.com

✉ Zhongxiang Ding
hangzhoudzx73@126.com

✉ Paul M. Thompson
pthomp@usc.edu

[1] School of Automation and Information Engineering, Sichuan University of Science and Engineering, Zigong, People's Republic of China

[2] Imaging Genetics Center, Mark & Mary Stevens Institute for Neuroimaging and Informatics, University of Southern California, Marina del Rey, CA, USA

[3] Department of Radiology, Zhejiang Provincial People's Hospital, Hangzhou, People's Republic of China

Functional MRI (fMRI) is a non-invasive imaging technique, widely used for presurgical planning in patients with brain tumors (Stippich et al. 2007; Tieleman et al. 2009). By eliciting brain activation with specific tasks, a large body of studies have shown that fMRI can be used to localize eloquent functional areas before tumor surgery, such as primary motor cortex and language areas (Stippich et al. 2007; Tieleman et al. 2009). However, the successful localization of functional areas using fMRI largely depends on the careful design of task paradigms as well as patient cooperation in correctly performing the tasks. Especially for those suffering from aphasia, physical impairment or cognitive dysfunction, task-based fMRI may fail to identify relevant functional areas (Price and Friston 1999; Vlieger et al. 2004).

Unlike task-based fMRI, resting-state fMRI (rs-fMRI) requires no explicit tasks for participants and is therefore particularly useful in patients who are unable to perform tasks consistently or at all (Liu et al. 2009; Lee et al. 2013). The technique measures spontaneous blood oxygen level dependent (BOLD) fluctuations to identify spatially coherent patterns (Fox and Raichle 2007). These patterns - known as resting state networks (RSNs) - are involved in multiple perceptual and cognitive functions, which are similar, in some respects, to functional maps evoked by explicit tasks (Smith et al. 2009). More importantly, all the RSNs can be obtained using the same set of rs-fMRI data. The prominent advantages of rs-fMRI have attracted enormous attention and several studies have investigated its potential value for presurgical mapping (see a review from Shimony et al. 2009). Rs-fMRI offers comparable power to task-based fMRI - and even cortical stimulation mapping - in the detection of motor areas (Kokkonen et al. 2009; Liu et al. 2009; Zhang et al. 2009; Qiu et al. 2014), as well as language areas (Tie et al. 2014; Sair et al. 2016), suggesting that rs-fMRI is a promising tool to localize eloquent functional areas in presurgical planning.

Existing studies have made huge efforts to localize motor or language areas. Even so, identifying other perceptual and cognitive networks is also necessary to guide surgical resection and avoid neurocognitive deficits, such as visual field defects, as well as attention, memory and executive impairments (Chang et al. 2007; Vargo 2017). In one recent rs-fMRI study, Mitchell et al. used a multi-layer neural network technique to identify seven RSNs in six epileptic patients and seven patients with cerebral tumors (Mitchell et al. 2013). However, the accuracy of their method is sensitive to the number and separability of RSNs being identified, as well as to the signal to noise ratio of the images (Hacker et al. 2013). Moreover, the algorithm itself is likely to neglect regions participating in functional reorganization due to the tumor tissue. These problems could, in principle, be solved by independent component analysis (ICA), which does not requires *a priori* information and can separate noise and multiple RSNs simultaneously (Beckmann et al. 2005). Two main concerns about using ICA to localize RSNs are the choice of the number of independent components (ICs number or model order) and component candidates representing the RSNs. Recently, Huang et al. (2016) developed a MATLAB toolbox for individualized presurgical mapping of eloquent functional areas using ICA. For individual patients, this toolbox can estimate the optimal number of ICs and component candidates for a single RSN, e.g., the sensorimotor network or language network. However, the optimal number of ICs for identifying multiple RSNs simultaneously has not yet considered.

One aim of the present study was to investigate the presurgical localization of multiple RSNs from rs-fMRI data using ICA in patients with brain metastases. Based on the method of Huang et al. (2016), our study presents an improved automatic identification method to search for the optimal number of ICs, for multiple RSNs, as well as optimal component candidates in each individual patient. In total, seven well-defined RSNs were examined, including: the default mode network (DMN), executive control network (ECN), dorsal attention network (DAN), language network (LN), sensorimotor network (SMN), auditory network (AN) and visual network (VN). Our second aim was to evaluate the spatial shift in the seven RSNs in the patients. We hypothesized that each RSN might undergo a spatial shift, related to the tumor location. Besides, we further speculate that the spatial shift would be different across RSNs, especially between perceptual networks (SMN, AN and VN) and higher cognitive networks (DMN, ECN, DAN and LN), as prior studies have pointed out a functional dichotomy between these two types of networks (Corbetta and Shulman 2002; Jann et al. 2010; Ding et al. 2011).

Materials and methods

Participants

The study was performed according to the Declaration of Helsinki and approved by the medical ethics committee of Zhejiang Provincial People's Hospital, Hangzhou, China. All participants provided written informed consent prior to enrollment in the experiments. Twelve patients (11 males, mean age: 60.0 ± 8.3 years) with newly diagnosed brain metastatic tumors between September 2016 and April 2017 were recruited for this study. The inclusion criteria included: 1) age greater than or equal to 18 years; 2) no more than three metastases; 3) known primary tumor sites; 4) no history of brain surgery or other neurological disease (e.g., traumatic brain injury, stroke or other focal brain lesions). Out of 12 patients, seven patients had suffered from a single brain metastasis and five from two to three brain metastases. The primary tumor sites included the lung (11 patients) and rectum (1 patient). Demographic and clinical characteristics of brain metastases

are summarized in Table 1. In addition, 14 healthy control volunteers (9 males, mean age: 60.9 ± 10.9 years) were recruited from the staff of Zhejiang Provincial People's Hospital. The healthy subjects were interviewed to confirm having no gross brain abnormalities in brain MRI images, and having no history of neurological or psychiatric disorders. There was no statistically significant difference in age (p=0.8976, two-tailed Mann-Whitney U test) or sex between the two groups (p=0.1696, two-tailed Fisher's exact test).

Image acquisition

All MRI scans were performed on a 3.0-T MR scanner (Discovery 750; GE Healthcare, Milwaukee, WI) at Zhejiang Provincial People's Hospital, Hangzhou, China. Foam padding and earplugs were used to reduce head motion and scanner noise. For each subject, we performed a conventional MRI protocol, including T1-weighted imaging, T2-weight imaging, T2-weighted fluid-attenuated inversion recovery (FLAIR) imaging, and diffusion weighted imaging, for routine investigation. High-resolution T1-weighted structural images were acquired in the sagittal orientation by using a magnetization-prepared rapid gradient-echo sequence (repetition time [TR]/echo time [TE] = 6.652/2.928 ms, flip angle = 12°, field of view = 256 × 256 mm^2, in-plane matrix = 256 × 256, voxel size = 1 × 1 × 1 mm^3, no inter-slice gap, and 192 slices) for each subject. The rs-fMRI data were acquired by using an echo-planar-imaging sequence for a total of 210 volumes (TR/TE = 2000/30 ms, flip angle = 90°, field of view = 220 × 220 mm^2, in-plane matrix = 64 × 64, voxel size = 3.44 × 3.44 × 3.2 mm^3, no inter-slice gap, and 35 transverse slices). During the fMRI scan, subjects were instructed to keep their eyes closed, relax but not to fall asleep, and try to keep their head still.

Image preprocessing

Images were preprocessed using the toolbox for Data Processing & Analysis for Brain Imaging (DPABI V2.3, http://rfmri.org/dpabi) (Yan et al. 2016). The first five functional images for each subject were excluded to ensure steady-state longitudinal magnetization. The remaining 205 consecutive volumes were corrected for temporal differences in acquisition and realigned to the first volume for head motion correction. No translation or rotation parameters in any subject exceeded 3 mm or 3°. Individual T1-weighted structural images were co-registered to the mean functional images after realignment, and then normalized to Montreal Neurological Institute (MNI) space. These transformation parameters were further applied for the normalization of functional images to MNI space with a resolution of 3 × 3 × 3 mm^3. For the patients, the presence of the tumor can cause distortions that affect the structural T1 image normalization, leading to bias when transforming the functional images. To avoid these distortions and optimize brain normalization, we used cost function masking (Brett et al. 2001; Andersen et al. 2010).

Table 1 Demographic and clinical characteristics of brain metastases

No.	Age/Sex	Metastasis number	Location	Size (mm^3)	Primary tumor
1	42/M	3	Right corpus callosum Left occipital Right occipital	1739 224 113	Lung
2	47/M	1	Right parieto-occipital	8040	Lung
3	63/M	1	Right occipital	66,977	Rectal
4	61/M	3	Left frontal Right frontal Right primary motor	4621 596 362	Lung
5	67/F	1	Right frontal	3026	Lung
6	68/M	1	Right primary motor	3056	Lung
7	67/M	1	Right frontal	1711	Lung
8	66/M	1	Left frontal	48	Lung
9	61/M	2	Right temporal Right cerebellum_8	144 3282	Lung
10	64/M	2	Left occipital Vermis_8	11,349 1228	Lung
11	60/M	3	Left parieto-occipital Left cerebellum_4_5 Left cerebellum_8	1211 2354 12,897	Lung
12	54/M	1	Left occipital	155	Lung

Specifically, each tumor was manually delineated on each slice of the T1-weighted anatomical images under the guidance of T2-weighted FLAIR images using MRIcron software (https://www.nitrc.org/projects/mricron). Next, a tumor mask was created by binarizing the tumor image and inverting it to yield zeros in the tumor and ones outside the tumor. The binary inverted tumor mask was then used as an input-weighting mask during the step of T1 images normalization to avoid effects of distortions caused by the tumor (Brownsett et al. 2014; Gooijers et al. 2016). After spatial normalization, we visually inspected the structural T1 images and functional images to ensure no potential image distortions existed due to the presence of tumor for each patient. Finally, the normalized functional images were spatially smoothed using a 6 mm full-width at half-maximum (FWHM) Gaussian kernel to attenuate spatial noise.

For each patient, tumor boundary was manually traced again on the normalized structural T1 images to generate a volume of interest. The corresponding volume was defined as tumor size, which may be found in Table 1. A population-based probability map about the distribution of tumors in the brain was also produced, and was presented in Supplementary Fig. 1.

Independent component analysis

In the control group, rs-fMRI data was analyzed using the group ICA of the fMRI toolbox (MICA, http://www.nitrc.org/projects/cogicat/) (Zhang et al. 2010). In this toolbox, the group ICA could be implemented multiple times with randomized initial values and different subject orders to achieve robust ICA results (Zhang et al. 2010). First, the optimal ICs number was estimated to be 40 using the minimum description length (MDL) criterion (Li et al. 2007). Then, we performed group ICA 25 times with random initial values and subject orders to obtain 40 ICs using the Infomax algorithm (Bell and Sejnowski 1995). Finally, the ICs' spatial maps were converted into z-score maps and a threshold at $z \geq 1.65$ (corresponding to a p value <0.05) was applied.

For the patients, single subject ICA - not group ICA - was performed on the rs-fMRI data to reveal spatial distributions of ICs, which is important for individualized presurgical mapping. To obtain the optimal number of ICs in an individual patient, we performed ICA using different ICs numbers ranging from 30 to 65, in increments of 5 (Huang et al. 2016). For each "number of ICs" setting, the ICA algorithm was repeated 25 times with random initial values using the Infomax algorithm. The ICs' spatial maps were further converted into z-score maps with a threshold at $z \geq 1.65$ (corresponding to a p value <0.05). The optimal ICs number was determined where the components of interest could be effectively identified as stated below.

Identification of RSNs

Identification of components using traditional visual inspection is experience-dependent and time-consuming, especially when the components are large. To reduce the time and labor for visual inspection of a total of 4600 components (controls: 40 ICs; patients: 380 ICs × 12 subjects), a template-matching-based automatic component identification method was performed using the 'discriminability index' (DI) as a quantitative similarity index (Huang et al. 2016). The larger the DI value is, the more similar the component is to the template. The RSN templates from Shirer et al. (2012) (http://findlab.stanford.edu/functional_ROIs.html) were used in this study. Briefly, we first binarized each component by using a threshold at $z \geq 1.65$ combining minimum cluster size of 20 voxels for each "number of ICs" setting. DI was then computed by comparing the binarized components with a RSN templates (e.g., SMN) as follows (Huang et al. 2016):

$$DI = z(\textit{hit}\ \text{rate}) - z(\textit{false}\ \text{alarm rate}),$$

where the *hit rate* is defined as the number of correctly identified voxels within a component divided by the total number of voxels in the RSN template; the *false alarm rate* is calculated as the number of mistakenly identified voxels within a component divided by the number of voxels outside the RSN template; $z(\cdot)$ refers to z-transformation. For each "number of ICs" setting, we ranked all components in a descending order according to their DI value and chose the first two components as candidates. By repeating these processes, we obtained the candidates for all RSNs, including the DMN (dorsal and ventral), ECN (left and right), DAN, LN, SMN, AN and VN (higher and primary).

For the control subjects, the group components representing each RSN were confirmed by visually inspecting the candidate components by two experienced researchers (J.R.D. and Z.D.) and then combined to produce the seven RSNs (DMN, ECN, DAN, LN, SMN, AN and VN) for the subsequent analyses.

To obtain the optimal number of ICs and presurgical RSN maps for individual patients, we proposed an improved automatic identification method based on a recent study (Huang et al. 2016). Specifically, the DI values of the first candidate for each RSN across all "number of ICs" settings were ranked in a descending order. The candidates with the first three DI values and those with the last three DI values were considered as the "good" and "bad" candidates for this RSN, respectively. Then, the optimal ICs number was determined where more RSNs had the "good" candidates and less RSNs had the "bad" candidates (Fig. 1). The optimal components representing each RSN were further confirmed by visually inspecting the candidates under the optimal "number of ICs" setting, and also combined to construct the seven RSNs.

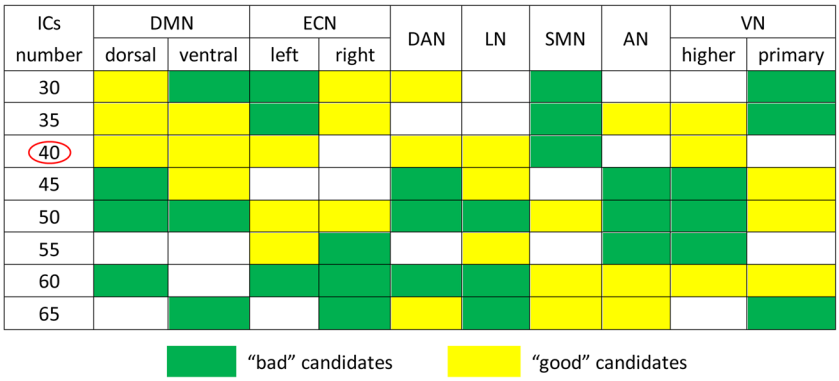

Fig. 1 Schematic for selecting the optimal number of ICs for multiple RSNs in each individual patient. Yellow blocks refer to "good candidates" - the components with the three largest DI values across "number of ICs" settings for a certain RSN. Green blocks represent "bad candidates" which are the components with the three smallest DI values across "number of ICs" settings for a certain RSN. Under the "number of ICs" setting of 40, more RSNs (here are six) have the "good" candidates and less RSNs (here is only one) have the "bad" candidates, so the optimal ICs number is 40 for this patient

Evaluation of spatial shift for RSNs mapping

Taking the RSNs from control subjects as contrasts, we evaluated the spatial shift of RSN maps in each patient, at both the RSN level and the regional level, by using the following two measures:

(1) Peak location shift

For a region within a RSN, the peak location shift was calculated as the Euclidean distance between the regional peak voxels from individual patients and controls:

$$D_i^X = \sqrt{\left(x_{ipatient} - x_{icontrols}\right)^2 + \left(y_{ipatient} - y_{icontrols}\right)^2 + \left(z_{ipatient} - z_{icontrols}\right)^2}, i \in X,$$

where i refers to a region within the RSN X, and (x,y,z) mean the MNI coordinates of the peak voxel in the region i.

Since each RSN usually includes several remote brain regions, it may be biased to evaluate the RSN location shift by only using the peak voxel's location within this RSN. Therefore, the peak location shift for a RSN was computed as the averaged regional peak location shift:

$$D^X = \left\langle D_i^X \right\rangle_{i \in X},$$

where $\langle\rangle$ denotes the mean across all regions within the RSN X. The peak location shift varied from zero. The larger this measure is, the more different the peak location of a region or RSN between individual patients and controls is.

(2) Spatial range shift

We first assessed the spatial similarity between the RSN maps from individual patients and controls using Dice coefficient (i.e., percentage overlap) (Tie et al. 2014; Sair et al. 2016). Then, the regional range shift and RSN range shift were separately defined as:

$$Range\ shift^i = 1 - Dice^i = 1 - \frac{2 \times V^i_{overlap}}{V^i_{patient} + V^i_{controls}},$$

$$Range\ shift^X = 1 - Dice^X = 1 - \frac{2 \times V^X_{overlap}}{V^X_{patient} + V^X_{controls}},$$

where i refers to a region within a RSN, X represents a RSN, $V_{patient}$ and $V_{controls}$ are the number of voxels within a region or a RSN from individual patients and controls, respectively, and $V_{overlap}$ is the number of overlapped voxels within a region or a RSN from both individual patients and controls. The spatial range shift varied between zero and one: it is zero if the voxels of a region or RSN in individual patients have the same size and location to those in controls which means no spatial range shift, and is one if there are no common voxels.

Results

Identification of RSNs

In the control group, the seven common RSNs were successfully identified from the group components using the template-matching-based automatic component identification method. The spatial distributions of the RSNs, shown in Fig. 2, are consistent with those reported in previous rs-fMRI studies (Damoiseaux et al. 2006; Ding et al. 2011; Shirer et al. 2012). These RSNs were used as the contrasts to evaluate the spatial shift of RSNs in individual patients, and a list of the brain regions within each RSN, along with the peak MNI coordinates and the associated cluster size, are reported in Table 2.

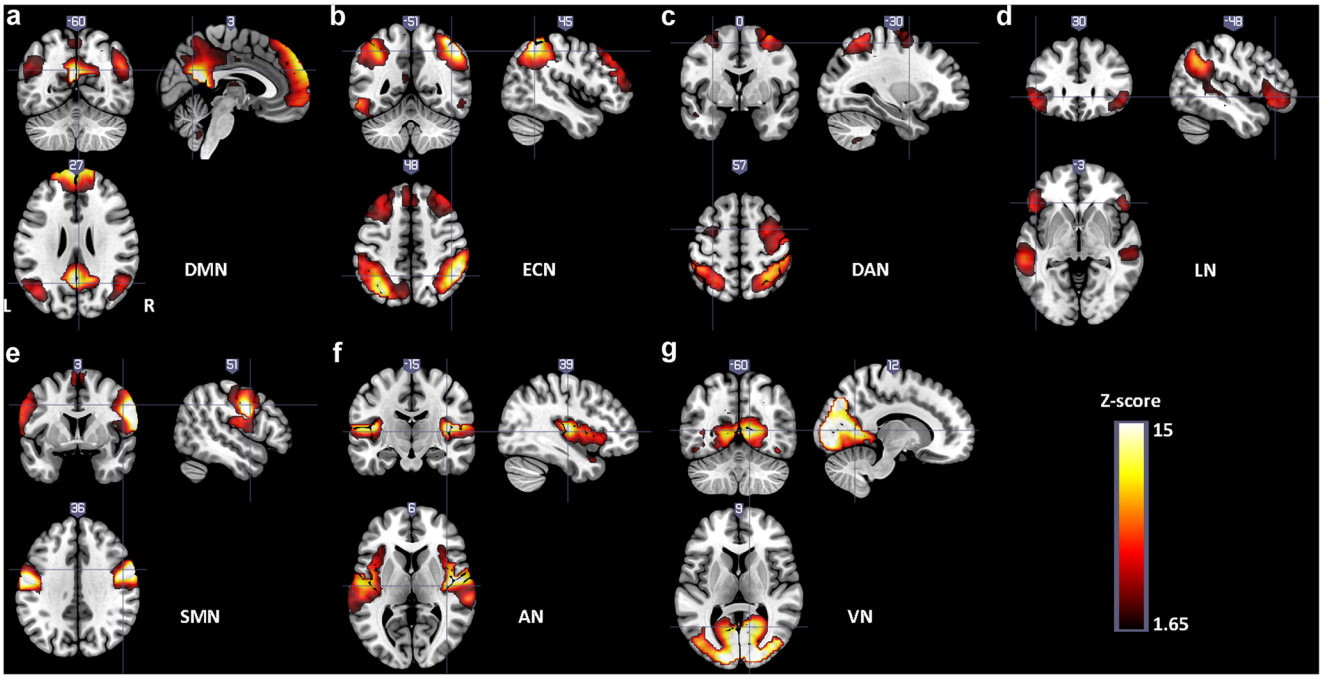

Fig. 2 Spatial distributions of the seven RSNs derived from a group analysis of rs-fMRI data in control subjects. The threshold was set at $z \geq 1.65$ (corresponding to a p value <0.05) combining minimum cluster size of 20 voxels. See Table 2 for coordinate details. L, left; R, right.

Using DI values as the quantitative evaluation index, we obtained the optimal number of ICs for each patient, which ranged from 40 to 65. Under the optimal "number of ICs" setting of individual patients, we also successfully identified the components representing the seven RSNs in all patients (Supplementary Fig. 2–8). The degree of overlap, for each RSN, across patients is shown in Fig. 3. On the whole, the distribution of RSNs identified in the patients was similar to that of RSN contrasts from controls.

Spatial shifts of RSNs

We quantitatively evaluated the spatial shift of each RSN in the patients based on the peak location shift and spatial range shift. Compared to the RSN contrasts from controls, the patients showed obvious shift in the peak location for each RSN (DMN: 17.4 ± 5.6, ECN: 20.0 ± 6.1, DAN: 23.9 ± 6.2, LN: 20.4 ± 7.8, SMN: 20.4 ± 9.8, AN: 16.6 ± 4.2, VN: 20.8 ± 4.9), as well as the spatial range (DMN: 0.449 ± 0.162, ECN: 0.493 ± 0.099, DAN: 0.596 ± 0.123, LN: 0.552 ± 0.074, SMN: 0.468 ± 0.096, AN: 0.447 ± 0.112, VN: 0.264 ± 0.089) (Fig. 4). We used one-way ANOVA to test the significant differences of spatial shift across RSNs; then we tested the significant difference between higher cognitive networks (DMN, ECN, DAN and LN) and perceptual networks (SMN, AN and VN) by a two-way ANOVA. There was a significant difference of the spatial range shift across RSNs, and the spatial range shifts in higher cognitive networks were significantly larger than those in perceptual networks ($F_{(1,22)}$=19.56, p<0.0001) (Fig. 4). There was no significant difference in the peak location shift across RSNs or between higher cognitive and perceptual networks ($F_{(1,22)}$=0.5373, p<0.4664).

Correlations between RSNs spatial shift and tumor location

It is important to know whether the RSNs' spatial shift is associated with tumor location in patients with brain metastases. Thus, the associations between spatial shift and the distance of tumor boundary-to-RSN were evaluated by using Spearman correlations (Schwarzkopf et al. 2012). First, we defined the distance of tumor boundary-to-region as the shortest Euclidean distance between the tumor boundary and the peak voxel of a region within an RSN contrast. Then, the distance of tumor boundary-to-RSN was computed as the shortest distance of tumor boundary-to-region across all regions within a RSN.

As seen in Fig. 5, the spatial range shift showed a negative correlation with the distance of tumor boundary-to-region in the right insula, ventromedial prefrontal cortex and middle occipital gyrus, while a positive correlation in the left frontal eye field and right postcentral gyrus (p<0.05). For the peak location shift, one region (the right Heschl's gyrus) and five regions (the left posterior cingulate cortex/precuneus, posterior inferior parietal lobule, inferior frontal gyrus, and right

Table 2 Cluster localization of RSNs identified in the control group

Regions	L/R	Peak MNI coordinates			Cluster size	Peak Z value
		X	Y	Z		
Default mode network (DMN)						
Ventromedial prefrontal cortex (vmPFC)	L	−3	60	33	1485	16.13
	R	3	63	30	1173	14.40
Posterior cingulate cortex (PCC)/precuneus (PCUN)	L	0	−54	18	572	22.29
	R	3	−51	15	549	20.49
Posterior inferior parietal lobule (pIPL)	L	−39	−69	39	243	13.63
	R	51	−60	30	301	8.97
Middle temporal gyrus (MTG)	L	−45	−66	24	342	5.50
	R	51	−60	24	319	6.50
Executive control network (ECN)						
Dorsolateral prefrontal cortex (dlPFC)	L	−48	24	33	1233	9.80
	R	42	33	39	1160	8.30
Dorsomedial prefrontal cortex (dmPFC)	L	0	39	33	354	5.54
	R	3	39	30	223	5.60
Anterior inferior parietal lobule (aIPL)	L	−30	−69	48	1256	15.08
	R	48	−48	54	1216	19.37
Inferior temporal gyrus (ITG)	L	−57	−54	−12	216	9.74
	R	60	−42	−9	64	5.60
Dorsal attention network (DAN)						
Frontal eye field (FEF)	L	−33	−6	66	163	4.05
	R	33	0	63	675	9.29
Intraparietal sulcus (IPS)	L	−48	−39	57	683	10.43
	R	30	−54	60	755	14.13
Middle temporal area (MT+)	L	−54	−69	6	136	3.18
	R	54	−60	0	85	4.48
Language network (LN)						
Frontal gyrus (IFG)	L	−54	21	0	226	7.03
SupraMarginal gyrus (SMG)	L	−57	−51	33	136	13.57
	R	60	−45	33	213	7.22
Angular gyrus (AG)	L	−54	−54	33	297	14.27
	R	57	−48	36	72	7.36
Superior temporal gyrus (STG)	L	−63	−51	24	98	7.02
	R	48	−27	−3	96	4.05
Middle temporal gyrus (MTG)	L	−57	−57	24	819	11.03
	R	57	−24	−6	157	4.73
Sensorimotor network (SMN)						
Precentral gyrus (PreCG)	L	−57	−6	33	365	18.23
	R	57	0	27	620	26.26
Rolandic operculum (ROL)	L	−63	−6	12	99	10.62
	R	63	−3	12	315	19.54
Supplementary motor area (SMA)	L	0	6	63	122	6.22
	R	3	6	69	67	5.18
Postcentral gyrus (PoCG)	L	−57	−9	36	627	18.64
	R	57	0	30	431	25.91
Auditory network (AN)						
Insula (INS)	L	−39	−21	15	350	14.97
	R	45	−9	9	419	18.35

Table 2 (continued)

Regions	L/R	Peak MNI coordinates			Cluster size	Peak Z value
		X	Y	Z		
Heschl's gyrus (Hes)	L	−42	−18	12	72	17.17
	R	48	−9	9	67	18.00
Superior temporal gyrus (STG)	L	−54	−24	12	598	16.17
	R	51	−24	18	574	15.32
Middle temporal gyrus (MTG)	L	−54	−30	9	311	8.70
	R	63	−33	6	57	6.77
Visual network (VN)						
Calcarine fissure (Cal)	L	−6	−93	0	536	26.10
	R	15	−90	0	522	30.64
Cuneus (CS)	L	0	−78	33	326	24.29
	R	15	−90	9	334	26.01
Lingual gyrus (LING)	L	0	−81	3	556	20.41
	R	15	−87	−3	623	26.82
Superior occipital gyrus (SOG)	L	−12	−93	3	231	21.60
	R	18	−93	6	262	24.32
Middle occipital gyrus (MOG)	L	−12	−96	3	609	22.78
	R	24	−90	6	386	18.45
Inferior occipital gyrus (IOG)	L	−15	−96	−6	237	19.61
	R	21	−90	−3	228	21.87

Abbreviations: *L* left, *R* right

anterior inferior parietal lobule and precentral gyrus) presented a negative and positive correlation with the distance of tumor boundary-to-region ($p<0.05$), respectively. At the RSN level, no correlation was found between the spatial range or peak location shift of a RSN and the distance of tumor boundary-to-RSN.

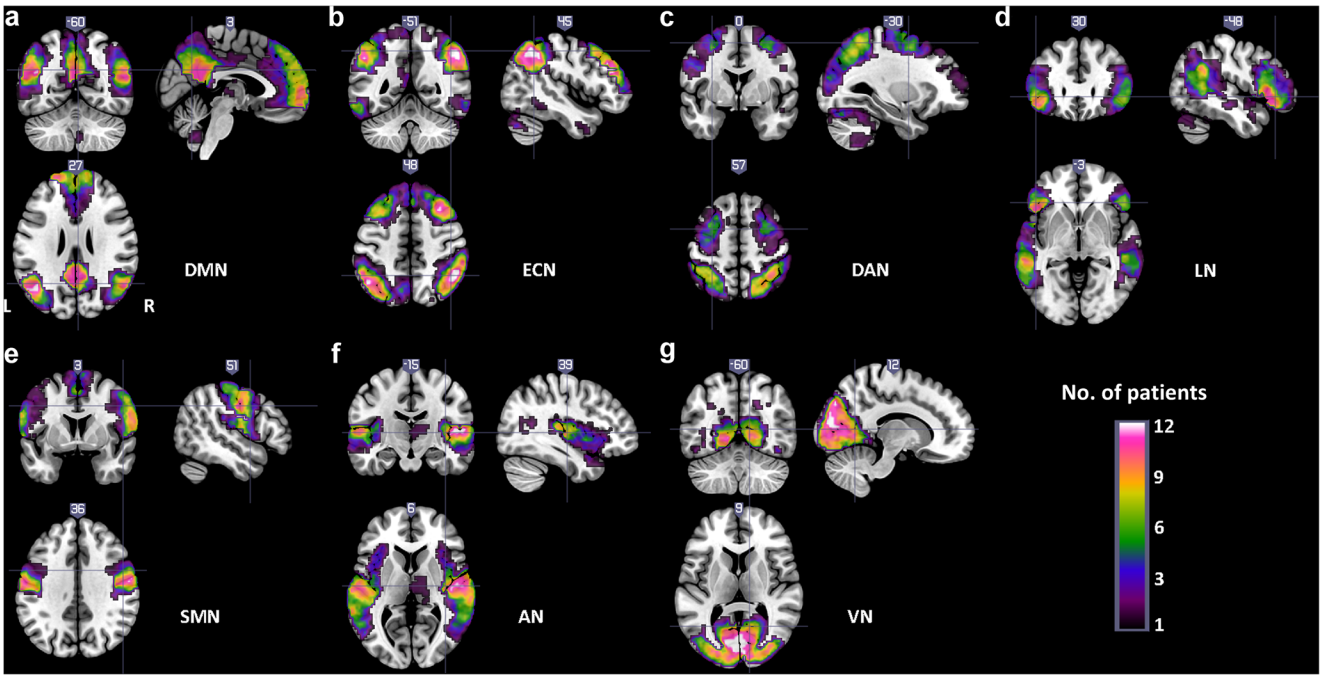

Fig. 3 Degree of RSNs overlap across all 12 patients with brain metastases. The colour code represents the number of patients in a given voxel. L, left; R, right.

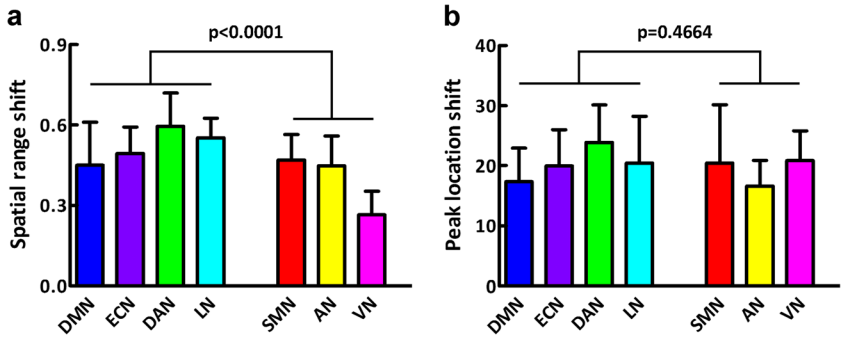

Fig. 4 Statistical analysis of spatial shift for higher cognitive and perceptual networks in patients with brain metastases. The group of higher cognitive networks includes DMN, ECN, DAN and LN; the group of perceptual networks includes SMN, AN and VN. **a** spatial ranges shift of RSNs; **b** peak location shift of RSNs. Error bars correspond to standard deviation. The *p* value is obtained by two-way ANOVA

Discussion

In this study, we investigated the presurgical localization of seven common RSNs from rs-fMRI data using ICA in patients with brain metastases. Combining our automatic identification method and visual inspection, we found that ICA could readily and reliably localize these RSNs from rs-fMRI data on an individual level. In addition, we found that each RSN had a

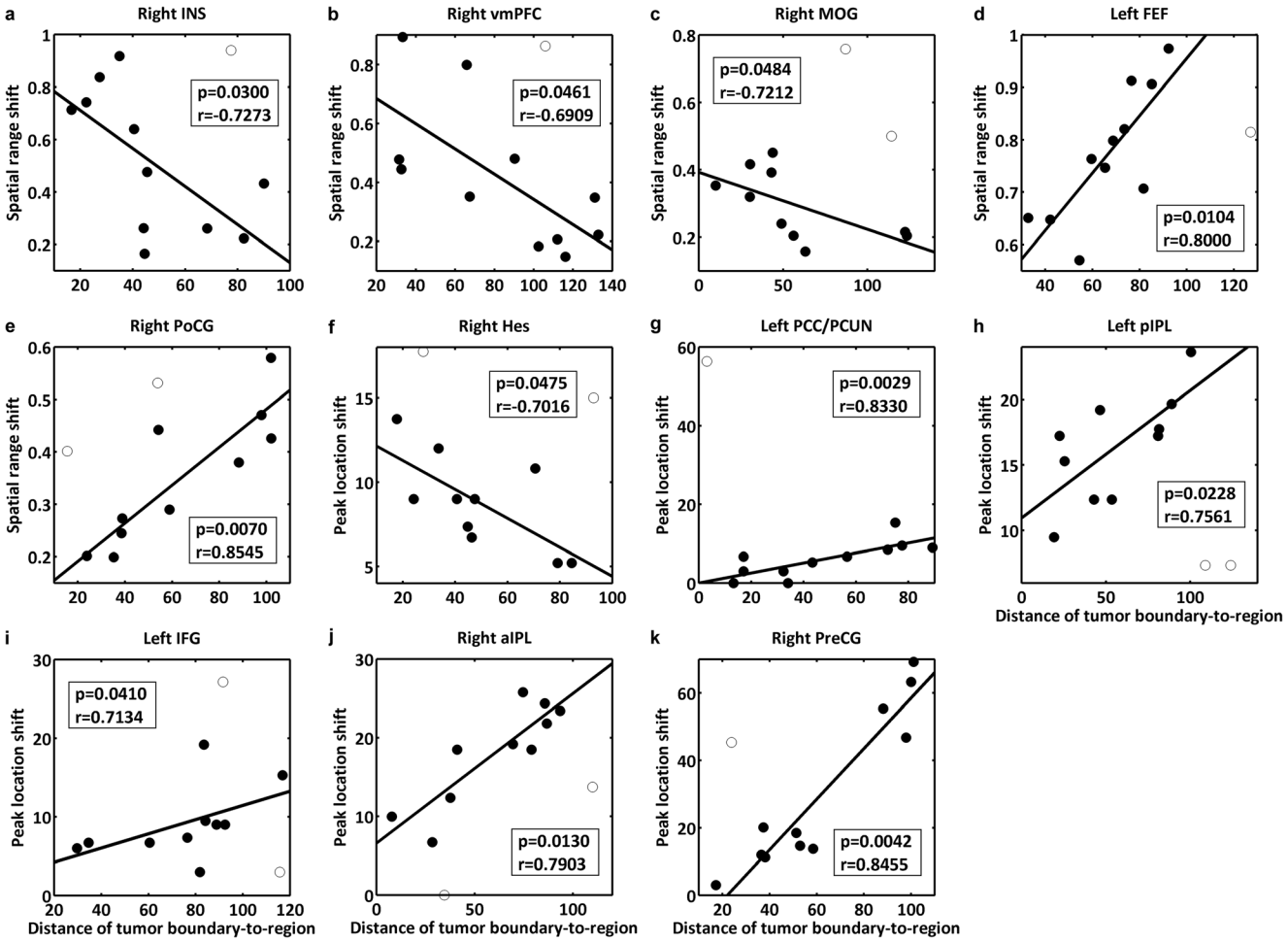

Fig. 5 Relationship of the regions spatial range shift and peak location shift to the distance of tumor boundary-to-region. Spearman correlations were computed over the data after removing outliers marked by circles. The significant level of correlation was set at $p<0.05$. INS, insula; vmPFC, ventromedial prefrontal cortex; MOG, middle occipital gyrus; FEF, frontal eye field; PoCG, postcentral gyrus; Hes, Heschl's gyrus; PCC/PCUN, posterior cingulate cortex/precuneus; pIPL, posterior inferior parietal lobule; IFG, inferior frontal gyrus; aIPL, anterior inferior parietal lobule; PreCG, precentral gyrus

visible spatial shift in each individual patient, and the spatial shift of some regions within RSNs was associated with the tumor location. Besides, there was a significant difference in spatial shift between perceptual and higher cognitive networks.

Reliability of identifying RSNs from individual patients' rs-fMRI data using ICA

There are several common RSNs in the brain, which are related to sensory, motor, language and cognitive functions (Rosazza and Minati 2011; Smith et al. 2013). Although surgical resection of metastases can extend survival time, it may also result in some neurocognitive deficits, such as aphasia, motor deficits, visual field defects, as well as attention, memory and executive impairments (Chang et al. 2007; Vargo 2017). Thus, it may be of crucial importance to map those RSNs for individualized presurgical planning (Zhang et al. 2009). The rs-fMRI technique enables us to obtain multiple RSNs in the same scanning data and requires no tasks, which is of great value for clinical application (Shimony et al. 2009; Lee et al. 2013).

ICA is a predominant approach used to extract RSNs from rs-fMRI (Lee et al. 2013). Unlike seed-based analysis, ICA performs a blind separation and doesn't require any prior assumptions (Beckmann et al. 2005). Group ICA has been generally applied to localize RSNs in healthy subjects (Damoiseaux et al. 2006; Liao et al. 2010b; Ding et al. 2011), and in brain disorders without obvious structural abnormalities such as mental disorders (Liao et al. 2010a; Yu et al. 2011; Qi et al. 2012). Similarly, we successfully localized the seven RSNs (DMN, ECN, DAN, LN, SMN, AN and VN) in control subjects, which were consistent with previous rs-fMRI studies (Damoiseaux et al. 2006; Ding et al. 2011; Shirer et al. 2012).

However, group ICA is not suitable for mapping RSNs in patients with structural changes, such as tumors or lesions (Kokkonen et al. 2009). Therefore, we performed ICA individually to localize RSNs in patients, since brain metastases differed in location, number and size in our study (Table 1). For individual ICA in patients, subject-specific ICs number may potentially improve the results which is valuable for presurgical mapping. Although the MDL criteria have been widely used for determining the optimal number of ICs (Li et al. 2007; Ding et al. 2011; Tie et al. 2014), we still need to be cautious in using it for individualized presurgical mapping. To obtain the optimal number of ICs for a specific subject, Huang et al. performed ICA analysis with multiple "number of ICs" settings in an individual patient and searched for the optimal component representing a RSN according to DI values (Huang et al. 2016). This method is useful for single RSN identification but not for localizing multiple RSNs simultaneously. In the present study, we used an improved automatic identification method based on the study of Huang et al. (2016) to automatically select the optimal number of ICs and component candidates for multiple RSNs in individual patients. Combined with visual inspection, our method reliably identified the seven RSNs for each patient with less burden in terms of choosing component candidates. The spatial distributions of RSNs in each patient were similar, but with some alterations relative to those identified in control subjects. Based on our findings, ICA based on rs-fMRI shows evidence of effectiveness and reliability for mapping RSNs in individual patients (Zhang et al. 2009; Tie et al. 2014), which may aid to individualized presurgical planning.

RSNs spatial shift and its association with tumor location

Brain tumors usually distort brain anatomy and associated functional areas, and thereby lead to shifts in functional networks in patients (Sunaert 2006; Qiu et al. 2014). Thus, to explore the shift of RSNs is potentially valuable for surgical resection to minimize the risk of irreversible postoperative neurocognitive impairments. Taking the RSNs from control subjects as contrasts, we quantitatively evaluated the spatial shift of RSNs in patients with brain metastases. We found that each RSN exhibited an obvious spatial shift in both peak location and spatial range, which could be also visualized based on the distribution maps of the RSNs in the individual patients. The existence of a tumor may disrupt synchronization between the region of damage and other connected regions within a network (Martino et al. 2011; Esposito et al. 2012), − this may manifest as less or no activation of some regions within a RSN determined by ICA. Meanwhile, a brain tumor can also trigger the spatial reorganization of functional networks by increasing activation of some component regions, or by inducing or moderating participation from other regions, such as motor, language and attention networks (Duffau 2001; Shinoura et al. 2006; Briganti et al. 2012; Charras et al. 2015). Therefore, our findings of RSNs spatial shift reflect the disruptions and reorganizations of functional networks in patients with brain metastases. Furthermore, the spatial shift showed significant correlations with the distance of tumor boundary-to-region in several regions within RSNs. It is reasonable that negative correlations were found between them in some regions. The functional regions will be less influenced when the tumor is far from them; otherwise some functional impairments will occur. The findings from Wood et al. (2011) showed that motor and language deficits increased as the distance from tumor to corresponding functional areas decreased. Surprisingly, the spatial shift in several regions was positively correlated with the distance of tumor boundary-to-region. As mentioned above, patients with brain tumors may have a quite

complicated functional disruptions, with complex reorganizations in functional networks. This may explain why both negative and positive correlations were found between spatial shift and the distance of tumor boundary-to-region. In short, the spatial shift of RSNs as well as correlations with tumor location reflect the complicated functional mechanism in patients with brain metastases, suggesting that the spatial shift of RSNs should be given more attention before surgical resection.

Prior studies in healthy subjects suggest a functional dichotomy between perceptual and higher cognitive networks (Corbetta and Shulman 2002; Jann et al. 2010; Ding et al. 2011), which can be partially explained by the different anatomical and connectional properties (Mesulam 1998). Brain metastases influence brain anatomy and functional connections, making it of interest to check whether spatial shift is different between the two groups of networks. Indeed, we found that higher cognitive networks (DMA, ECN, DAN and LN) showed a significantly larger spatial range shift than perceptual networks (SMN, AN and VN) in patients with brain metastases. Higher cognitive networks participate in complex cognitive processes including memory, attention, language, executive control and consciousness (Mesulam 1998), which involve more brain regions; information processing in these networks may also be more complex than for perceptual networks. So, it is not surprising that the spatial range shift is larger in higher cognitive networks compared to perceptual networks under pathologic conditions. Besides, there was no significant difference in peak location shift between the two groups of RSNs indicating that peak location shift is not marker to reflect different RSNs. Our results suggest that the dichotomy between perceptual and higher cognitive networks does not only exist in normal cognitive functions but also in pathologic alterations due to metastases.

Methodological considerations and study limitations

Our study should be interpreted in the light of several methodological considerations. First, the choice of optimal ICs number depends on more RSNs having the "good" candidates (the three largest DI values) and less RSNs having the "bad" candidates (the three smallest DI values) (as seen in Fig. 1). Under this optimal "number of ICs" setting, the component representing a certain RSN is inevitably not the optimal one. If certain RSNs are of special concern, appropriate weight coefficients can be considered to select the optimal number of ICs. Second, the RSNs range is threshold dependent, so we calculated the distance of tumor boundary-to-RSN as the shortest distance between tumor boundary and the peak voxel of regions within RSNs rather than the RSNs boundary. Third, the DMN, ECN and VN are generally split into two parts using ICA, such as dorsal and ventral DMN, left and right ECN, higher and primary VN. In this study, the two parts were combined to form one RSN; this may obscure the changes within each part, but has no influence on the localization of the RSNs.

The current study has some limitations. The first limitation is the small sample size of patients: our improved component identification method based on ICA should be tested in more patients with metastatic disease. Due to the small sample size, the reason for the different spatial range shift between higher cognitive networks and perceptual networks could be secondary to site and volume of the brain metastatic lesion. Thus, the dichotomy of spatial shift between the two groups of networks also needs to be verified in a larger sample size in future study. The second limitation is the biased sex proportion of patients with brain metastases. Eleven out of 12 patients were men, perhaps because ~92% of the primary tumors were lung tumors in this study. The results should be interpreted carefully as it is unclear whether sex differences may affect the spatial shift in RSNs. Another limitation is that we did not differentiate patients with functional deficits from those without functional deficits due to the limited sample size. Subgroup analyses may help us to better understand the functional disruptions and reorganizations due to metastases. Despite these limitations, this study presents a potential solution to identify multiple RSNs in individual patients, and the results are promising.

Conclusions

In conclusion, we used an improved component automatic identification method to localize seven common RSNs in patients with brain metastases. The successful localization suggests that ICA can effectively and reliably identify RSNs from rs-fMRI data in individual patients. The RSNs identified in the patients exhibited an obvious spatial shift and the spatial shift of some regions correlated with tumor location, which may reflect functional disruptions and reorganizations due to metastases. Moreover, there was a significant difference of spatial shift between perceptual and higher cognitive networks, suggesting a functional dichotomy between the two groups of networks even in pathologic alterations caused by metastases.

Acknowledgements This work was supported by the National Natural Science Foundation of China (No. 81401482) and the Educational Commission of Sichuan Province of China (No. 17ZA0269). P. Thompson is funded in part by the NIH, under grant U54 EB020403 from the Big Data to Knowledge (BD2K) program.

Compliance with ethical standards

Conflict of interest The authors declare that they have no conflict of interest.

Ethical approval All procedures performed in studies involving human participants were in accordance with the ethical standards of the institutional and/or national research committee and with the 1964 Helsinki declaration and its later amendments or comparable ethical standards.

Informed consent Informed consent was obtained from all individual participants included in the study.

References

Andersen, S. M., Rapcsak, S. Z., & Beeson, P. M. (2010). Cost function masking during normalization of brains with focal lesions: still a necessity? *NeuroImage, 53*, 78–84.

Beckmann, C. F., DeLuca, M., Devlin, J. T., & Smith, S. M. (2005). Investigations into resting-state connectivity using independent component analysis. *Philosophical Transactions of the Royal Society of London. Series B, Biological Sciences, 360*, 1001–1013.

Bell, A. J., & Sejnowski, T. J. (1995). An information-maximization approach to blind separation and blind deconvolution. *Neural Computation, 7*, 1129–1159.

Brett, M., Leff, A. P., Rorden, C., & Ashburner, J. (2001). Spatial normalization of brain images with focal lesions using cost function masking. *NeuroImage, 14*, 486–500.

Briganti, C., Sestieri, C., Mattei, P. A., Esposito, R., Galzio, R. J., Tartaro, A., et al. (2012). Reorganization of functional connectivity of the language network in patients with brain gliomas. *AJNR - American Journal of Neuroradiology, 33*, 1983–1990.

Brownsett, S. L., Warren, J. E., Geranmayeh, F., Woodhead, Z., Leech, R., & Wise, R. J. (2014). Cognitive control and its impact on recovery from aphasic stroke. *Brain : a Journal of Neurology, 137*, 242–254.

Chang, E. L., Wefel, J. S., Maor, M. H., Hassenbusch 3rd, S. J., Mahajan, A., Lang, F. F., et al. (2007). A pilot study of neurocognitive function in patients with one to three new brain metastases initially treated with stereotactic radiosurgery alone. *Neurosurgery, 60*, 277–283 discussion 283–274.

Charras, P., Herbet, G., Deverdun, J., de Champfleur, N. M., Duffau, H., Bartolomeo, P., et al. (2015). Functional reorganization of the attentional networks in low-grade glioma patients: a longitudinal study. *Cortex; a Journal Devoted to the Study of the Nervous System and Behavior, 63*, 27–41.

Corbetta, M., & Shulman, G. L. (2002). Control of goal-directed and stimulus-driven attention in the brain. *Nature Reviews Neuroscience, 3*, 201–215.

Damoiseaux, J. S., Rombouts, S. A., Barkhof, F., Scheltens, P., Stam, C. J., Smith, S. M., et al. (2006). Consistent resting-state networks across healthy subjects. *Proceedings of the National Academy of Sciences of the United States of America, 103*, 13848–13853.

Delattre, J. Y., Krol, G., Thaler, H. T., & Posner, J. B. (1988). Distribution of brain metastases. *Archives of Neurology, 45*, 741–744.

Ding, J. R., Liao, W., Zhang, Z., Mantini, D., Xu, Q., Wu, G. R., et al. (2011). Topological fractionation of resting-state networks. *PLoS One, 6*, e26596.

Duffau, H. (2001). Acute functional reorganisation of the human motor cortex during resection of central lesions: a study using intraoperative brain mapping. *Journal of Neurology, Neurosurgery, and Psychiatry, 70*, 506–513.

Esposito, R., Mattei, P. A., Briganti, C., Romani, G. L., Tartaro, A., & Caulo, M. (2012). Modifications of default-mode network connectivity in patients with cerebral glioma. *PLoS One, 7*, e40231.

Fox, M. D., & Raichle, M. E. (2007). Spontaneous fluctuations in brain activity observed with functional magnetic resonance imaging. *Nature Reviews Neuroscience, 8*, 700–711.

Gavrilovic, I. T., & Posner, J. B. (2005). Brain metastases: epidemiology and pathophysiology. *Journal of Neuro-Oncology, 75*, 5–14.

Gooijers, J., Beets, I. A., Albouy, G., Beeckmans, K., Michiels, K., Sunaert, S., et al. (2016). Movement preparation and execution: differential functional activation patterns after traumatic brain injury. *Brain : a Journal of Neurology, 139*, 2469–2485.

Hacker, C. D., Laumann, T. O., Szrama, N. P., Baldassarre, A., Snyder, A. Z., Leuthardt, E. C., et al. (2013). Resting state network estimation in individual subjects. *NeuroImage, 82*, 616–633.

Huang, H., Ding, Z., Mao, D., Yuan, J., Zhu, F., Chen, S., et al. (2016). PreSurgMapp: a MATLAB toolbox for presurgical mapping of eloquent functional areas based on task-related and resting-state functional MRI. *Neuroinformatics, 14*, 421–438.

Jann, K., Kottlow, M., Dierks, T., Boesch, C., & Koenig, T. (2010). Topographic electrophysiological signatures of FMRI Resting State Networks. *PLoS One, 5*, e12945.

Kokkonen, S. M., Nikkinen, J., Remes, J., Kantola, J., Starck, T., Haapea, M., et al. (2009). Preoperative localization of the sensorimotor area using independent component analysis of resting-state fMRI. *Magnetic Resonance Imaging, 27*, 733–740.

Lee, M. H., Smyser, C. D., & Shimony, J. S. (2013). Resting-state fMRI: a review of methods and clinical applications. *AJNR - American Journal of Neuroradiology, 34*, 1866–1872.

Li, Y. O., Adali, T., & Calhoun, V. D. (2007). Estimating the number of independent components for functional magnetic resonance imaging data. *Human Brain Mapping, 28*, 1251–1266.

Liao, W., Chen, H., Feng, Y., Mantini, D., Gentili, C., Pan, Z., et al. (2010a). Selective aberrant functional connectivity of resting state networks in social anxiety disorder. *NeuroImage, 52*, 1549–1558.

Liao, W., Mantini, D., Zhang, Z., Pan, Z., Ding, J., Gong, Q., et al. (2010b). Evaluating the effective connectivity of resting state networks using conditional Granger causality. *Biological Cybernetics, 102*, 57–69.

Lin, X., & DeAngelis, L. M. (2015). Treatment of brain metastases. *Journal of Clinical Oncology: Official Journal of the American Society of Clinical Oncology, 33*, 3475–3484.

Liu, H., Buckner, R. L., Talukdar, T., Tanaka, N., Madsen, J. R., & Stufflebeam, S. M. (2009). Task-free presurgical mapping using functional magnetic resonance imaging intrinsic activity. *Journal of Neurosurgery, 111*, 746–754.

Martino, J., Honma, S. M., Findlay, A. M., Guggisberg, A. G., Owen, J. P., Kirsch, H. E., et al. (2011). Resting functional connectivity in patients with brain tumors in eloquent areas. *Annals of Neurology, 69*, 521–532.

Mesulam, M. M. (1998). From sensation to cognition. *Brain : a Journal of Neurology, 121*(Pt 6), 1013–1052.

Mitchell, T. J., Hacker, C. D., Breshears, J. D., Szrama, N. P., Sharma, M., Bundy, D. T., et al. (2013). A novel data-driven approach to preoperative mapping of functional cortex using resting-state functional magnetic resonance imaging. *Neurosurgery, 73*, 969–982 discussion 982–963.

Price, C. J., & Friston, K. J. (1999). Scanning patients with tasks they can perform. *Human Brain Mapping, 8*, 102–108.

Qi, R., Zhang, L. J., Xu, Q., Zhong, J., Wu, S., Zhang, Z., et al. (2012). Selective impairments of resting-state networks in minimal hepatic encephalopathy. *PLoS One, 7*, e37400.

Qiu, T. M., Yan, C. G., Tang, W. J., Wu, J. S., Zhuang, D. X., Yao, C. J., et al. (2014). Localizing hand motor area using resting-state fMRI: validated with direct cortical stimulation. *Acta Neurochirurgica, 156*, 2295–2302.

Rosazza, C., & Minati, L. (2011). Resting-state brain networks: literature review and clinical applications. *Neurological Sciences : Official Journal of the Italian Neurological Society and of the Italian Society of Clinical Neurophysiology, 32*, 773–785.

Sair, H. I., Yahyavi-Firouz-Abadi, N., Calhoun, V. D., Airan, R. D., Agarwal, S., Intrapiromkul, J., et al. (2016). Presurgical brain mapping of the language network in patients with brain tumors using resting-state fMRI: comparison with task fMRI. *Human Brain Mapping, 37*, 913–923.

Schwarzkopf, D. S., De Haas, B., & Rees, G. (2012). Better ways to improve standards in brain-behavior correlation analysis. *Frontiers in Human Neuroscience, 6*, 200.

Shimony, J. S., Zhang, D., Johnston, J. M., Fox, M. D., Roy, A., & Leuthardt, E. C. (2009). Resting-state spontaneous fluctuations in brain activity: a new paradigm for presurgical planning using fMRI. *Academic Radiology, 16*, 578–583.

Shinoura, N., Suzuki, Y., Yamada, R., Kodama, T., Takahashi, M., & Yagi, K. (2006). Restored activation of primary motor area from motor reorganization and improved motor function after brain tumor resection. *AJNR - American Journal of Neuroradiology, 27*, 1275–1282.

Shirer, W. R., Ryali, S., Rykhlevskaia, E., Menon, V., & Greicius, M. D. (2012). Decoding subject-driven cognitive states with whole-brain connectivity patterns. *Cerebral Cortex, 22*, 158–165.

Sills, A. K. (2005). Current treatment approaches to surgery for brain metastases. *Neurosurgery, 57*, S24–S32 discusssion S21–24.

Smith, S. M., Fox, P. T., Miller, K. L., Glahn, D. C., Fox, P. M., Mackay, C. E., et al. (2009). Correspondence of the brain's functional architecture during activation and rest. *Proceedings of the National Academy of Sciences of the United States of America, 106*, 13040–13045.

Smith, S. M., Vidaurre, D., Beckmann, C. F., Glasser, M. F., Jenkinson, M., Miller, K. L., et al. (2013). Functional connectomics from resting-state fMRI. *Trends in Cognitive Sciences, 17*, 666–682.

Stippich, C., Blatow, M., & Karkow, K. (2007). Presurgical functional MRI in patients with brain tumors. In C. Stippich (Ed.), *Clinical functional MRI: Presurgical functional neuroimaging* (pp. 87–134). Berlin, Heidelberg: Springer.

Sunaert, S. (2006). Presurgical planning for tumor resectioning. *Journal of Magnetic Resonance Imaging : JMRI, 23*, 887–905.

Tie, Y., Rigolo, L., Norton, I. H., Huang, R. Y., Wu, W., Orringer, D., et al. (2014). Defining language networks from resting-state fMRI for surgical planning–a feasibility study. *Human Brain Mapping, 35*, 1018–1030.

Tieleman, A., Deblaere, K., Van Roost, D., Van Damme, O., & Achten, E. (2009). Preoperative fMRI in tumour surgery. *European Radiology, 19*, 2523–2534.

Vargo, M. M. (2017). Brain tumors and metastases. *Physical Medicine and Rehabilitation Clinics of North America, 28*, 115–141.

Vlieger, E. J., Majoie, C. B., Leenstra, S., & Den Heeten, G. J. (2004). Functional magnetic resonance imaging for neurosurgical planning in neurooncology. *European Radiology, 14*, 1143–1153.

Wood, J. M., Kundu, B., Utter, A., Gallagher, T. A., Voss, J., Nair, V. A., et al. (2011). Impact of brain tumor location on morbidity and mortality: a retrospective functional MR imaging study. *AJNR - American Journal of Neuroradiology, 32*, 1420–1425.

Yan, C. G., Wang, X. D., Zuo, X. N., & Zang, Y. F. (2016). DPABI: data processing & analysis for (resting-state) brain imaging. *Neuroinformatics, 14*, 339–351.

Yu, Q., Plis, S. M., Erhardt, E. B., Allen, E. A., Sui, J., Kiehl, K. A., et al. (2011). Modular organization of functional network connectivity in healthy controls and patients with Schizophrenia during the resting state. *Frontiers in Systems Neuroscience, 5*, 103.

Zhang, D., Johnston, J. M., Fox, M. D., Leuthardt, E. C., Grubb, R. L., Chicoine, M. R., et al. (2009). Preoperative sensorimotor mapping in brain tumor patients using spontaneous fluctuations in neuronal activity imaged with functional magnetic resonance imaging: initial experience. *Neurosurgery, 65*, 226–236.

Zhang, H., Zuo, X. N., Ma, S. Y., Zang, Y. F., Milham, M. P., & Zhu, C. Z. (2010). Subject order-independent group ICA (SOI-GICA) for functional MRI data analysis. *NeuroImage, 51*, 1414–1424.